Mathematical Biosciences and Engineering

MBE, 16(6): 7510–7525.
DOI: 10.3934/mbe.2019377
Received: 16 May 2019
Accepted: 09 August 2019
Published: 19 August 2019

http://www.aimspress.com/journal/MBE

Research article

Identification on acidification damage of external anode system induced by impressed current cathodic protection for reinforced concrete

Jie Hu[1], Yangyang Wang[1], Yuwei Ma[2,*], Jiangxiong Wei[1] and Qijun Yu[1]

[1] School of Materials Science and Engineering, South China University of Technology, Guangzhou 510640, PR China
[2] Guangzhou University-Tamkang University Joint Research Center for Engineering Structure Disaster Prevention and Control, Guangzhou University, Guangzhou 510006, China

* **Correspondence:** Email: yuwei.ma@hotmail.com; Tel: +862039337975; Fax: +862039337975.

Abstract: Impressed current cathodic protection (ICCP) was widely applied for the corrosion control of reinforced concrete. During the ICCP treatment, the anodic reactions happened on the primary anode surface may induce acidification and subsequently pH drop in the vicinity of the anode, leading to damage of the external anode mortar. In this study, the relationship between the applied current (simulating ICCP treatment) on the Ti mesh anode and pH alterations in simulated concrete pore (SCP) solution (with/without chlorides) was investigated. It was found that the applied current slightly reduced the corrosion resistance of Ti mesh; this negative effect was more pronounced in the presence of chlorides. The pH value of SCP solution near Ti mesh anode decreased when the external current was applied. The consumption rate of OH^- ion was higher in the chloride-containing SCP solution. A mathematical model was proposed between the electric charge quantity (Q) and OH^- concentration (cOH^-) in SCP solution near Ti mesh anode. This model is a useful tool to quantitatively identify the acidification damage induced by impressed current from the perspective of pH alternation near Ti mesh anode.

Keywords: impressed current cathodic protection; acidification damage; pH alteration; mathematical model; external anode system

1. Introduction

In recent years, due to the rapid development of coastal economy and increased exploitation of marine resources, reinforced concrete structures are increasingly used in severe marine environment all over the world. The chloride penetration in marine environment results in severe corrosion damage of the reinforcement, which significantly influences the durability and service life of construction structures [1]. It is well known that corrosion damage (especially pitting corrosion) influences the mechanical properties of the reinforcement [2]. Further, the accumulation of corrosion products (with a volume several times larger than that of the original reinforcement [3,4]) leads to strain on the concrete in the vicinity of the reinforcement and subsequently cracking and spalling of the concrete cover, thus reducing the bonding strength between the reinforcement/concrete interface and bearing capacity of the reinforced concrete (due to the reduced cross-sectional area of the reinforcement) [1,5,6]. Therefore, the application of efficient techniques to prevent and repair corrosion damage of reinforced concrete structures in marine environment is of great importance.

So far, various techniques were proposed and applied for the corrosion control of reinforced concrete, including coatings, corrosion inhibitors and electrochemical protection techniques [7–9]. Among them, impressed current cathodic protection (ICCP) was widely investigated and applied [10], because it can directly halt the electrochemical corrosion reaction of the steel reinforcement. When ICCP is applied for reinforced concrete structures, the steel reinforcement is cathodically polarized (with an instant off potential in the range from –720 mV to –1100 mV vs. Ag/AgCl/0.5 M KCl reference electrode [11]). Under this condition, the dissolution of the steel reinforcement is inhibited, and the corrosion reaction is thermodynamically halted [12]. Besides the cathodic polarization of the reinforcement, ICCP technique also provides several other benefits [13,14]: it results in an increased alkalinity and reduced chloride concentration at the steel/concrete interface, leading to a positive shift of pitting potential and enlarged passivation potential range for the reinforcement; in addition, ICCP treatment maintains the high alkaline environment at the steel/concrete interface, resulting in a more stable passive layer on the steel surface. Therefore, when enough cathodic protection current is applied, ICCP can provide a long-term corrosion protection for reinforced concrete structures [15]).

In order to guarantee the uniform distribution of the protective current, external anode system is applied on concrete surface for ICCP treatment. The external anode system is normally consisted of activated Ti mesh as the primary external anode and conductive mortar as the secondary anode [13]. When ICCP is applied for reinforced concrete, the following anodic reactions will occur at the vicinity of the external Ti mesh anode [16]:

$$4OH^- \rightarrow O_2 + 2H_2O + 4e^- \quad (1)$$

$$2H_2O \rightarrow O_2 + 4H^+ + 4e^- \quad (2)$$

In marine environment, when chlorides penetrate into the mortar and reach Ti mesh surface, the following anodic reactions will also occur [16]:

$$2Cl^- \rightarrow Cl_2 + 2e^- \quad (3)$$

$$Cl_2 + 2OH^- \rightarrow Cl^- + ClO^- + H_2O \quad (4)$$

The above anodic reactions continuously consume OH^- in mortar pore solution near Ti mesh anode, leading to subsequently dissolution of hydration products and more porous microstructure of

cement matrix at Ti mesh/mortar interface (known as acidification process), which reduces the durability of the external anode system. In addition, during the acidification process, the alteration of mineral composition and microstructure of the mortar also negatively influences the conductivity of external anode mortar and uniform distribution of the protective current [17], and thus the stable operation of ICCP treatment. Therefore, it is very important to investigate and evaluate the process of acidification damage in the external anode mortar.

At present, the investigation on the acidification damage of the external anode system under the applied external current was mainly conducted with a high current density (about 1 A/m^2), namely electrochemical chloride extraction (ECE). Carmona et al. [10] found that pH value of the electrolyte near the anode decreased from 7 to 5.5 after ECE, and the possible reason may be related to the oxidation of OH^- or decomposition of water and carbonization. Bertolini et al. [18] found that cement matrix was destroyed in the vicinity of the primary anode due to the acidity generated by the anodic reactions after only 1–2 months ECE treatment.

Due to the low current density (5–20 mA/m^2 [11,19]), the acidification damage caused by ICCP treatment was seldom reported. McArthur [20] simulated the pH alteration and diffusion trend towards cathode in simulated pore solution with a current density of 20 mA/m^2. The results indicated that after 1050 h, the acidification area reached 260 mm in a glass tube with a cross section area of 4.9 mm^2. By using numerical simulation, Peelen et al. [21] found that with a current density of 1 mA/m^2, the acidification area was up to 100 μm after 10 years. Compared to ECE, the applied current density of ICCP is rather low (about 2–3 orders of magnitude lower); however, due to its long operation time [22], the acidification damage will definitely influence the durability and performance of the external anode mortar.

The acidification damage of the external anode mortar caused by the applied external current is a complex process, involving both the consumption of OH^- ion in pore solution and subsequently dissolution-precipitation of calcium hydroxide (CH, a typical hydration product in cement-based materials) in the vicinity of the primary anode [21]. Because the above acidification process initiates in pore solution of the external mortar, the objective of this study is to establish the relationship between the consumption rate of OH^- ion and quantity of electric charge during ICCP treatment. The electrochemical performance of Ti anode immersed in SCP solutions after ICCP treatment with different current densities was characterized by electrochemical measurements and surface analysis; pH alterations of SCP solutions (with/without chlorides) in the vicinity of the anode under different current densities were also determined. On the basis of the above experimental results, a mathematical model was proposed between the acidification damage near Ti mesh anode and quantity of electric charge during ICCP treatment from the perspective of pH alternation.

2. Materials and method

2.1. Sample preparations

2.1.1. Steel electrode and Ti mesh electrode

Q235 smooth construction steel bar (with a diameter of 14 mm and length of 30 mm) was used as the cathode and its chemical compositions are as follows: Fe 98.91%, C 0.18%, Si 0.28%, Mn 0.55%, S 0.04%, P 0.04%. The surface of the steel bar was successively ground and polished by

using 200#，600#，1000# and 2000# abrasive papers and then cleaned with ethanol. The working area of the prepared steel bar electrode was about 13.18 cm^2. The anode used in this study was Ti mesh with dimensions of 25 mm × 40 mm and surface area of 20.10 cm^2; the surface of Ti mesh was also cleaned with ethanol before tests.

2.1.2. Simulated concrete pore (SCP) solutions

According to the reported studies [23–27], SCP solution was prepared by 0.002 mol/l $Ca(OH)_2$ + 0.06 mol/l NaOH + 0.18 mol/l KOH, and its pH value was adjusted to 13 by 0.1 mol/l HNO_3 in this study (the initial OH^- concentration in SCP solution was 0.1 mol/l). In addition, 3.5 wt. % NaCl was added in SCP solution, simulating the chloride-contaminated environment. The reagents used for the preparation of SCP solutions were analytical pure.

2.1.3. Experimental set-up

40 ml SCP solution (chloride-free or chloride-containing SCP solution) was filled into two separate wide-mouth bottles to simulate the cathodic area (cathode cell) and anodic area (anode cell), respectively. The galvanostat (Corrtest CS1002, China) was used as the external power supply to provide the external protective current: the steel bar (cathode) and Ti mesh (anode) was connected to the negative and positive terminal of the power supply, respectively. The efficient electrical connection between the solutions in two bottles was guaranteed by salt bridge. The applied current density used in this study was 100 mA/m^2 and 200 mA/m^2 (based on the surface area of the steel reinforcement), respectively, which was about 10 times higher than the normally used current density for ICCP (5–20 mA/m^2 [11,19]). The purpose for using such high current densities is to accelerate the acidification caused by the applied external current and to shorten the experimental cycle (similar current density was also used in the reported study on cathodic protection [28]). Meanwhile, the reference specimen without the applied external current was also prepared. The sample designations in this study are as follows: Specimens Ref, S100 and S200 were specimens immersed in the chloride-free SCP solution and with the current density of 0 mA/m^2, 100 mA/m^2 and 200 mA/m^2, respectively; specimens Cl-Ref, Cl-S100 and Cl-S200 were specimens immersed in the chloride-containing SCP solution and with the current density of 0 mA/m^2, 100 mA/m^2 and 200 mA/m^2, respectively.

2.2. Methods

2.2.1. Electrochemical measurements

After 15 days of ICCP treatment, the applied external current was turned off and electrochemical measurements were conducted when the open circuit potential (OCP) of Ti mesh anode was stable. The equipment used was 273A potentiostat/galvanostat (EG&G PAR, Oak Ridge, TN, USA) and 5210 lock-in amplifier system. The electrochemical measurements performed in this study included electrochemical impedance spectroscopy (EIS) and potentio-dynamic polarization (PDP). A conventional three-electrode set-up was used: Ti mesh as working electrode (WE), saturated calomel electrode (SCE) as reference electrode (RE) and Ti mesh as counter electrode (CE). The scanning potential range for PDP was –0.2–1.0 V vs. OCP, with a scanning rate of 0.5 mV/s. EIS

measurements were carried out at OCP and in a frequency range from 100 kHz to 10 mHz.

2.2.2. Surface analysis of Ti mesh electrode

After the treatment, the morphology and composition of products formed on Ti mesh surface were examined by scanning electron microscopy (SEM, Zeiss Evo 18) and X-ray diffraction (XRD). SEM images (with magnifications of 150× and 2000×) were taken in secondary electron (SE) mode, using an accelerating voltage of 20 kV. XRD analysis was performed by scanning the surface of the specimens with a scan step of 0.0167°, by using PAN analytical X'pert Pro (Almelo, The Netherlands). The energy source was Cu K_α and the tube settings were 40 kV and 40 mA.

2.2.3. pH measurements of simulated concrete pore solutions

In order to monitor the acidification process in SCP solutions, 8–10 ml SCP solution in the anode cell was collected every 24 h to measure the pH value by using Mettler Toledo FE20K pH meter. The collected solution was re-filled to the original cell after each measurement. There were 3 replicates for each specimen.

3. Results

3.1. Effect of the applied external current on Ti mesh anode

3.1.1. Electrochemical behavior of Ti mesh anode after ICCP treatment

Figure 1 presents PDP curves of Ti mesh anode in SCP solutions after ICCP treatment (15 d). Due to its excellent corrosion resistance, Ti mesh presented the corrosion potential in the range of –0.133 V—0.281 V after ICCP treatment, indicating a low corrosion activity of Ti mesh during the treatment. However, the electrochemical performance of Ti mesh anode was still influenced by the applied external current. As shown in Figure 1, the corrosion potential of Ti mesh anode was negatively shifted under the applied external current, and a more negative corrosion potential was related to a higher applied current density. For example, in the chloride-containing SCP solution, when the external current was not applied, the corrosion potential of Ti mesh was –0.172 V; however the corrosion potential was shifted to –0.225 V and –0.267 V with a current density of 100 mA/m^2 and 200 mA/m^2, respectively. When the external current was applied, the anodic current density of Ti mesh was also increased and this negative effect was more pronounced with a higher applied current density. Additionally, when the same current density was applied, the anodic current density was higher in the chloride-containing SCP solution.

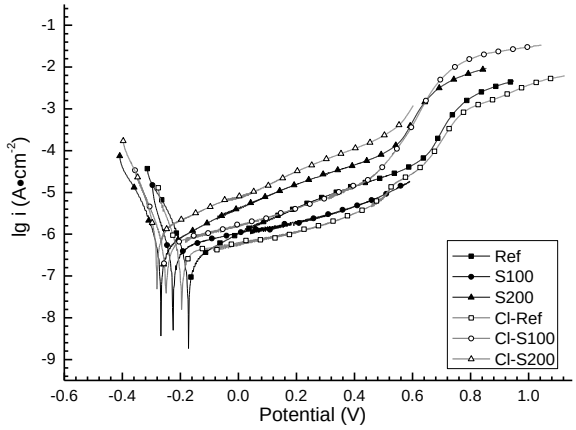

Figure 1. Potentio-dynamic polarization curves of Ti mesh anode after ICCP treatment (15 d).

The corrosion current densities (I_{corr}) for all specimens, calculated from PDP curves are given in Figure 2. Generally, a lower I_{corr} is corresponding to a better corrosion resistance of Ti mesh. When the external current was applied, I_{corr} of Ti mesh anode increased; Ti mesh presented a higher I_{corr} value with a higher applied current density (specimen Ref: 0.072 μA/cm^2; specimen S100: 0.157 μA/cm^2; specimen S200: 0.249 μA/cm^2). The above results indicated that the applied external current slightly reduced the corrosion resistance of Ti mesh in SCP solution. Further, it is also observed that the specimen immersed in chloride-containing SCP solution presented a higher I_{corr} value, compared to specimen immersed in chloride-free solution (e.g. specimen S200: 0.249 μA/cm^2; specimen Cl-S200: 0.478 μA/cm^2). It means that in marine environment, the negative effect of ICCP treatment on the electrochemical performance of Ti mesh was more pronounced. This effect was further confirmed by electrochemical impedance spectroscopy (EIS).

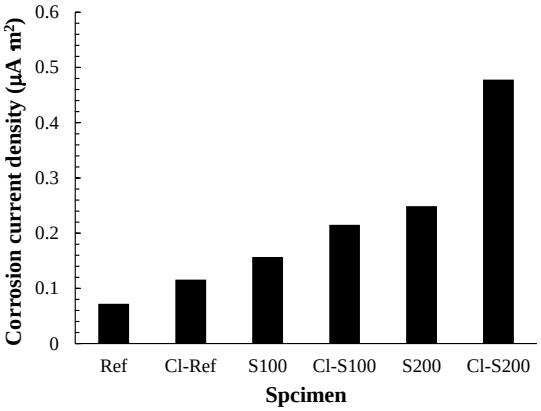

Figure 2. Corrosion current density of Ti mesh anode calculated based on PDP curves.

Figure 3 depicts EIS responses of Ti mesh anode after ICCP treatment (15 d). When the external current was applied, the magnitude of |Z| was reduced, indicating a lower corrosion resistance of Ti mesh anode; the reduction degree was more pronounced when a higher current density was applied. This negative effect was also evidenced by the slightly lower phase angle with the applied external

current (e.g. 83.9 ° for specimen Ref and 80.9 ° for specimen S200). Further, with the same current density, the magnitude of |Z| was even smaller in the chloride-containing SCP solution (also presenting a slightly lower phase angle: e.g., 79.4 ° for specimen Cl-S200 and 80.9 °for specimen S200), indicating an even lower corrosion resistance of Ti mesh anode in the presence of chlorides.

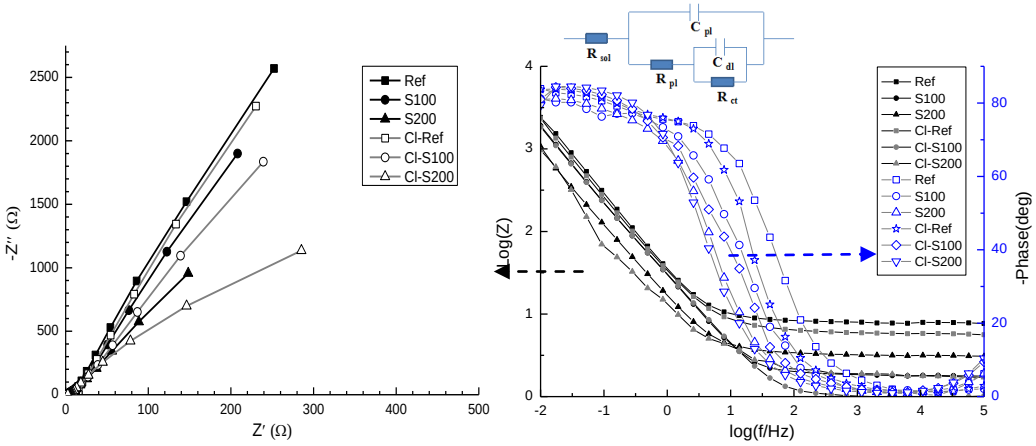

Figure 3. Electrochemical impedance spectroscopy of Ti mesh anode after ICCP treatment (15 d).

In this study, the experimental EIS responses were fitted by using an equivalent circuit ($R_{sol}(C_{pl}(R_{pl}(C_{dl}R_{ct}))$). The hereby used circuit is considered to sufficiently describe the electrochemical behavior of Ti mesh anode with a clear physical meaning for each parameter involved [29]: R_{sol} is the electrical resistance of SCP solutions; the first time constant (product layer capacitance C_{pl} and product layer resistance R_{pl}) is related to the property of the formed product layer; the second time constant (electric double layer capacitance C_{dl} and charge transfer resistance R_{ct}) is attributed to the electrochemical reaction on Ti mesh surface, including the charge transfer process in combination with the mass transport process.

The best fit parameters for all specimens are summarized in Table 1. When the external current was applied, the product layer resistance (R_{pl}) increased (e.g. specimen Ref: 751.64 $\Omega \cdot cm^2$; specimen S100: 1132.64 $\Omega \cdot cm^2$; specimen S200: 912.34 $\Omega \cdot cm^2$). The possible reason is as follows: when the external current was not applied, due to the high alkalinity of SCP solution, no obvious product was formed on the surface of Ti mesh anode, leading to a clean surface. However, when the external current was applied, the corrosion rate of Ti mesh was slightly accelerated, and corrosion product layer was formed on the surface of Ti mesh, leading to an increased R_{pl}. Further, a lower R_{pl} was related to a higher applied current density and chloride-containing SCP solution (e.g. specimen Cl-S100: 591.84 $\Omega \cdot cm^2$; specimen Cl-S200: 503.71 $\Omega \cdot cm^2$). Under the above situations (higher applied current density or in chloride-containing SCP solution), the corrosion resistance of Ti mesh was lower, leading to a more porous product layer with a reduced R_{pl} (the morphology and composition of product layer formed on the surface of Ti mesh are shown in Figure 4 and Figure 5 and will be discussed in detail in *Section 3.1.2* further below).

Table 1. Best fit parameters from experimental EIS results of Ti mesh anode after ICCP treatment (15 d).

Specimens	C_{pl} (μF/cm^2)	R_{pl} (Ω·cm^2)	C_{dl} (μF/cm^2)	R_p (kΩ·cm^2)
Ref	378.81	751.64	175.62	201.30
S100	416.92	1132.64	315.32	143.82
S200	868.96	912.34	606.57	54.56
Cl-Ref	342.99	436.07	269.95	165.42
Cl-S100	367.76	591.84	368.56	107.33
Cl-S200	158.71	503.71	894.53	38.22

When the external current was applied, a decrease of polarization resistance (R_p) was observed (e.g. specimen Ref: 201.30 kΩ·cm^2; specimen S100: 143.82 kΩ·cm^2; specimen S200: 54.56 kΩ·cm^2); in contrast, C_{dl} of Ti mesh anode increased with the applied external current (e.g. specimen Ref: 175.62 μF/cm^2; specimen S100: 315.62 μF/cm^2; specimen S200: 606.57 μF/cm^2). The results indicate that the corrosion resistance of Ti mesh anode was reduced when the external current was applied, especially with a higher current density. Further, when the same current density was applied, R_p value of Ti mesh anode was even lower in the chloride-containing SCP solution (e.g. specimen S200: 54.56 kΩ·cm^2; specimen Cl-S200: 38.22 kΩ·cm^2).

3.1.2. Surface analysis of Ti mesh anode after ICCP treatment

The surface morphologies of Ti mesh after ICCP treatment (15 d) are shown in Figure 4. In the chloride-free SCP solution, when the external current was not applied (Figure 4a), the surface of Ti mesh was smooth and clean, and no obvious product was observed; however, when the external current was applied (Figure 4b and c), certain amount of products was formed and accumulated on the surface of Ti mesh. The accumulation of products caused by the acidification effect was more severe with a higher current density. Further, the accumulation of products on Ti mesh surface in the chloride-containing SCP solution was more pronounced under the same applied current density, compared to the chloride-free SCP solution (Figure 4d).

The composition of Ti mesh surface after ICCP treatment (15 d) was examined by XRD, as shown in Figure 5. The products formed on the surface of Ti mesh were mainly TiO_2, corresponding to the peaks at 34.98 °, 37.09 °, 39.70 °, 51.88 °, 62.73 ° and 68.75 ° in XRD patterns. It was observed that in the chloride-free SCP solution, when the current was applied, the amount of TiO_2 increased, evidenced by the higher peak intensity at 39.70 °, 51.88 °, 62.73 °; further, the peaks corresponding to TiO_2 were more pronounced with a higher applied current density (specimen S200).

Similarly, in the chloride-containing SCP solution, a higher current density was also related to a more pronounced accumulation of products. Further, with the same current density, compared to the chloride-free SCP solution, the peaks corresponding to the accumulative products were more pronounced in the chloride-containing SCP solution, indicating that more products were formed on Ti mesh surface in the presence of chlorides.

The electrochemical measurements, combined with surface analysis indicate that although Ti mesh presents an excellent corrosion resistance in SCP solution (even in the presence of chlorides), the acidification caused by ICCP can still slightly reduce the corrosion resistance of Ti mesh, thus influencing the service life of Ti mesh anode and stable operation of ICCP.

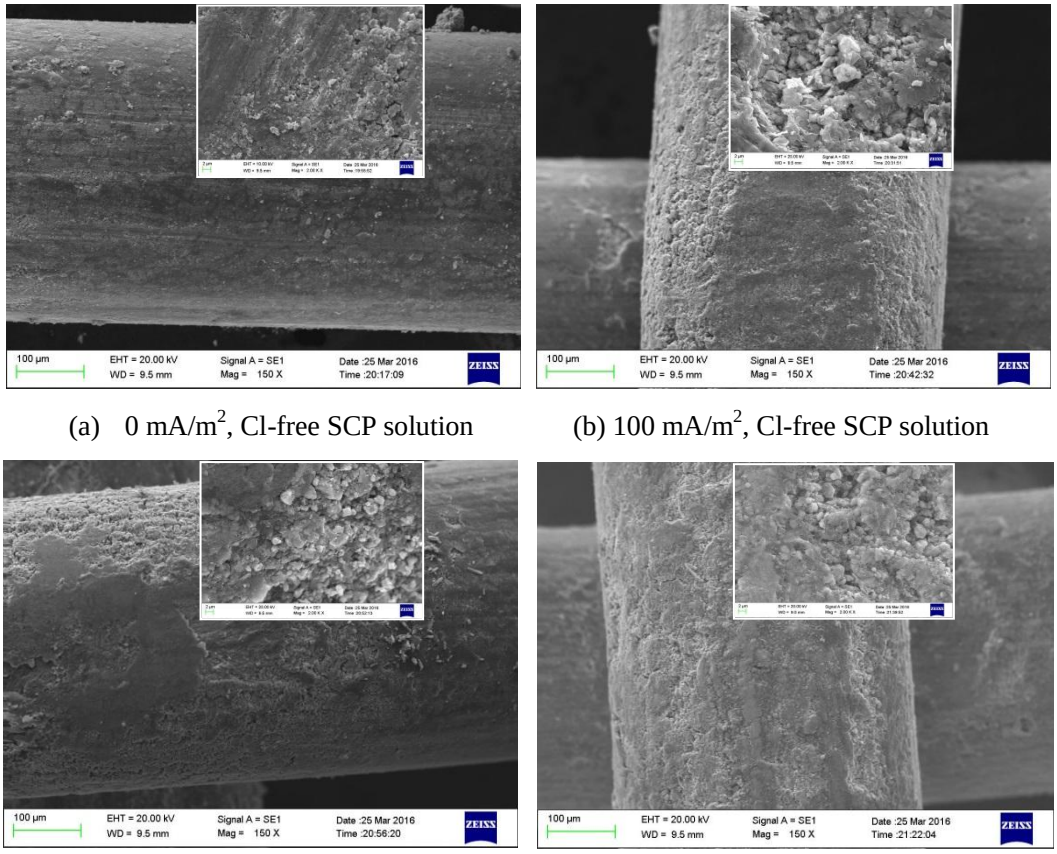

(a) 0 mA/m^2, Cl-free SCP solution (b) 100 mA/m^2, Cl-free SCP solution

(b) 200 mA/m^2, Cl-free SCP solution (d) 200 mA/m^2, Cl-containing SCP solution

Figure 4. Morphology of Ti mesh in SCP solutions after ICCP treatment (15 d).

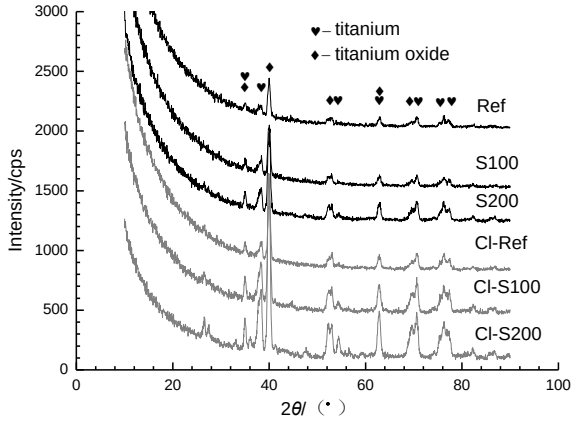

Figure 5. XRD results of the surface products formed on anodic Ti mesh after ICCP treatment (15 d).

3.2. Effect of the applied external current on simulated concrete pore solution in the anode cell

3.2.1. pH alterations of SCP solutions in the anode cell during ICCP treatment

pH alteration of SCP solutions in the anode cell during ICCP treatment is shown in Figure 6. pH

value of SCP solution in the anode cell significantly decreased with the applied external current: e.g. after 15 d, pH value decreased to 9.25 for the chloride-free SCP solution, and 9.45 for the chloride-containing SCP solution with a current density of 200 mA/m^2. pH value of SCP solution dropped to a smaller value when a higher current density was applied. For example, in the chloride-free SCP solution, pH value dropped to 9.25 with a current density of 200 mA/m^2, compared to 10.07 with a current density of 100 mA/m^2 after 15 d. When the applied current density increased, the electric charge amount and accordingly amount of the electrons through the external circuit also increased. Therefore, the consumption rate of OH^- caused by anodic reactions was accelerated under a higher current density, leading to a more pronounced reduction of pH value of SCP solution in the anode cell.

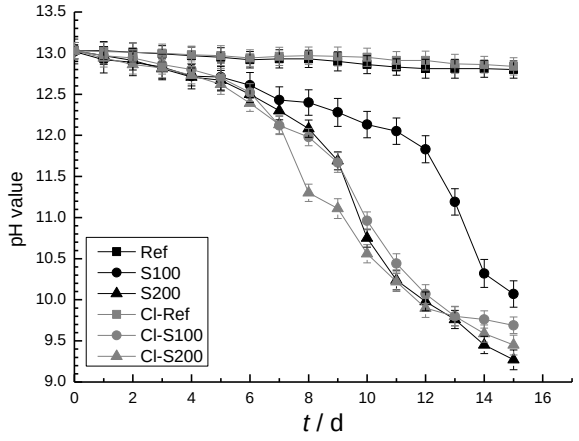

Figure 6. Effect of the applied external current on pH values of SCP solutions in the anode cell.

3.2.2. Alteration of OH- concentration in SCP solutions in the anode cell

After ICCP treatment for 15 d, the alteration of OH^- concentration (calculated based on the measured pH value) in SCP solutions in the anode cell is shown in Figure 7 (the maximum consumption rate of OH^- ion expressed by the differential result of the fitted curve is also shown in the figure). The higher maximum consumption rate of OH^- was related to the higher applied current density: compared to the specimens with a current density of 100 mA/m^2, when a current density of 200 mA/m^2 was applied, the maximum consumption rate was 23.84% higher in the chloride-free SCP solution and 8.33% higher in the chloride-containing SCP solution. Further, the maximum consumption rate of OH^- was higher in the presence of chlorides. For example, with an applied current density of 200 mA/m^2, the maximum consumption rate of OH^- was 0.0182 mol/(l d) in the chloride-containing SCP solution, which was higher than 0.0161 mol/(l d) in the chloride-free SCP solution. The results indicated that the applied external current reduced OH^- concentration in SCP solution in the anode cell and this harmful effect was more pronounced under the chloride-containing environment. Chlorides can accelerate the dissolution of Ti mesh, and the dissolved titanium ions can then combine with OH^- in SCP solution to form TiO_2 adsorbing on the surface of Ti mesh. Therefore, the decrease of OH^- concentration in SCP solution was more obvious. This explanation is evidenced by SEM and XRD analysis as shown in Figure 4 and Figure 5.

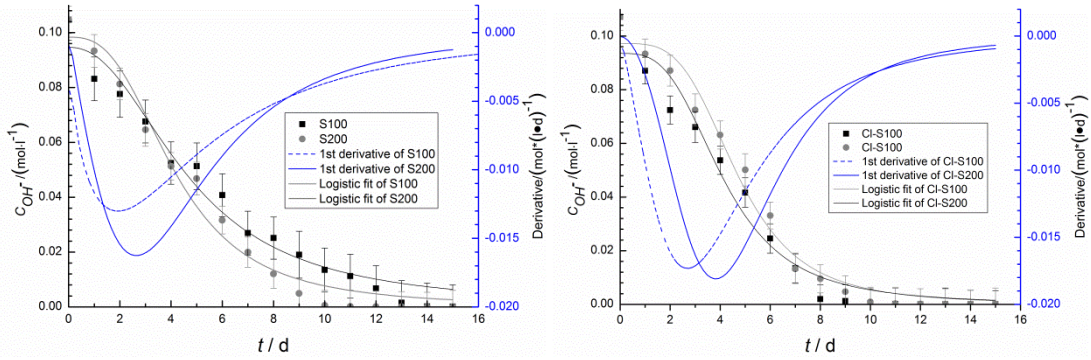

(a) Without chlorides (b) With chlorides

Figure 7. Relationship between OH^- concentration in SCP solution in the anode cell and treatment time under the applied external current.

4. Discussions

4.1.1. Comparison of the experimental and theoretically calculated consumption amounts of OH^- ion in SCP solutions under the applied external current

During ICCP treatment in this study, the accumulative electric charge quantity Q (C) can be described as the following equation:

$$Q=It \tag{5}$$

where I is the applied external current (A) and t is the treatment time (s).

The amount of the transferred electrons during the treatment can then be expressed as Eq 6:

$$n_{electrons}=\frac{Q}{F}=\frac{It}{F} \tag{6}$$

where F is Faraday constant (96485 C/mol electrons).

According to reactions (1)–(4), the consumed amount of OH^- in SCP solution equals to the amount of the transferred electrons in the external circuit. Therefore, the consumed amount of OH^- in SCP solution in the anode cell under the applied external current can be theoretically calculated by Eq 7:

$$n_{OH^-,in\ theoretical}= n_{electrons}=\frac{Q}{F}=\frac{It}{F} \tag{7}$$

Besides, the consumption amount of OH^- derived from the experimental measurements can be obtained by Eqs 8 and 9:

$$n_{OH^-,inexperimental}=n_{OH^-,initial}-n_{OH^-,t} \tag{8}$$

$$n_{OH^-}=V\times 10^{(pH-14)} \tag{9}$$

where $n_{OH^-,initial}$ is the initial OH^- amount in SCP solution (0.004 mol in this study); $n_{OH^-,t}$ is the OH^- amount in SCP solution corresponding to time t (s); V is the volume of SCP solution (0.04 l).

Table 2. The consumption amounts of OH^- in SCP solutions in the anode cell after ICCP treatment (15 d) derived both from the experimental measurements and theoretical calculation.

Specimen	Experimental results	Theoretical calculation	$n_{experimental}/n_{theoretical}$
S100	3.9953×10^{-3} mol	1.3538×10^{-3} mol	2.9512
S200	3.9993×10^{-3} mol	2.7076×10^{-3} mol	1.4771
Cl-S100	3.9998×10^{-3} mol	1.3538×10^{-3} mol	2.9545
Cl-S200	3.9999×10^{-3} mol	2.7076×10^{-3} mol	1.4773

Based on the above calculations, the experimental and theoretically calculated consumption amounts of OH^- in SCP solutions in the anode cell under the applied external current for 15 d are shown in Table 2. The results indicate that when the current was applied, the actual consumption amount of OH^- was significantly higher than the theoretically calculated value. When the applied current density was 100/200 mA/m^2, the actual consumption amount of OH^- was about 1.95/0.48 times higher, compared to the calculated values after 15 d. The possible reason for the difference in the experimental and calculated consumption amount of OH^- was as follows: when the external current was applied, the caused acidification consumed OH^- in SCP solution near Ti mesh, leading to a pH drop of SCP solution. Meanwhile, corrosion resistance of Ti mesh also slightly decreased after the pH drop of SCP solution. The dissolved titanium ions combined with OH^- in SCP solution nearby to form insoluble titanium hydroxide on the surface of Ti mesh. Finally, the insoluble titanium hydroxide maybe dehydrated and transferred to TiO_2 adsorbing on the surface of Ti mesh, evidenced by XRD analysis as shown in Figure 5. Therefore, the dissolution of Ti mesh and subsequently formation of surface products also consumed OH^- in SCP solution, leading to a higher consumption amount compared to the calculated values.

Because the above calculation based on the related anodic reactions is not able to reflect the real influence of the applied external current on the pH alteration of SCP solution in the anode cell, an alternative method to evaluate the acidification effect on OH^- concentration of SCP solution caused by ICCP treatment was proposed and discussed further below.

4.1.2. Relationship between OH^- concentration in SCP solutions and accumulative electric charge quantity during ICCP treatment

The relationship between the accumulative electric charge quantity during ICCP treatment and OH^- concentration of SCP solutions in the anode cell is shown in Figure 8. After fitting, the relationship between OH^- concentration in SCP solutions (c) and electric charge quantity (Q) is in accordance with Logistic regression model, as expressed in Eq 10:

$$c = \frac{c_0}{1 + \left(Q / Q_0\right)^P} \tag{10}$$

Where c is OH^- concentration in SCP solution in the anode cell (mol/l); c_0 is the initial OH^- concentration in SCP solution in the anode cell (0.1 mol/l in this study); Q is the accumulative electric charge quantity (C); Q_0 is the accumulative electric charge quantity at the turning point (the electric charge quantity corresponding to the highest consumption rate of OH^- in SCP solution, C); P is the regression coefficient. The fitting curves are also shown in Figure 8 and the related fitting parameters are shown in Table 3.

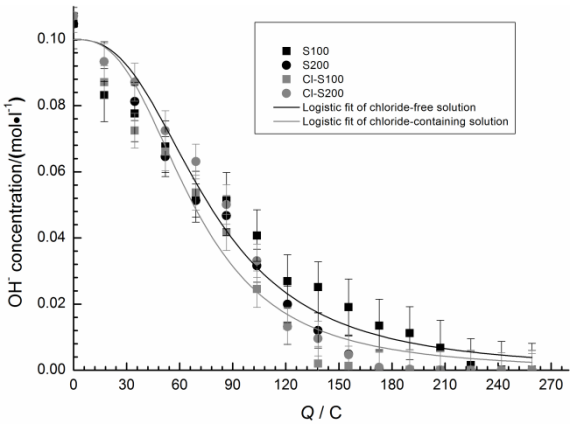

Figure 8. Relationship between OH^- concentration in SCP solution in the anode cell and accumulative electric charge quantity during ICCP treatment.

Table 3. Fitting parameters in the Logistic equation.

	Parameter	Value	Standard deviation	R^2
In chloride-free SCP solutions	c_0	0.100	0.000	
	Q_0	81.941	2.725	0.964
	P	2.365	0.178	
In chloride-containing SCP solutions	c_0	0.100	0.000	
	Q_0	72.319	2.446	0.966
	P	3.122	0.274	

It was observed in Table 3 that R^2 value for the fitting of the specimens in the chloride-free and chloride-containing SCP solution was 0.964 and 0.966, respectively, indicating that the correlation degree of this equation was high, and the fitting results were reliable.

Based on the above calculations and fittings, the relationship between OH^- concentration of the chloride-free SCP solution in the anode cell and accumulative electric charge quantity can be expressed as Eq 11:

$$c = \frac{c_0}{1+\left(Q/81.941\right)^{2.365}} \tag{11}$$

The relationship between OH^- concentration of the chloride-contaminated SCP solution in the anode cell and accumulative electric charge quantity can be expressed as equation (12):

$$c = \frac{c_0}{1+\left(Q/72.319\right)^{3.122}} \tag{12}$$

Therefore, the above equations can be used for quantitative calculation on OH^- concentration of SCP solution during ICCP treatment based on the accumulative electric charge quantity and potential evaluation on the acidification damage in the external anode mortar induced by ICCP treatment. It should be mentioned that the above Eqs (Eq 11 and 12) can only be used to evaluate the influence of the applied external current (simulating ICCP treatment) on OH^- concentration of SCP solutions near Ti mesh (with/without chlorides). In the external anode mortar, the acidification effect caused by the applied external current is much more complex: the dissolution of CH, which happens in the vicinity of Ti mesh anode, presents a buffering effect on pH value of pore solution, thus leading to a slow decrease rate of OH^- concentration of pore solution in the external anode mortar [17]. The above buffering effect was not relevant in this study (due to the testing medium, simulated concrete pore solution), thus the experiment results derived in this paper can't be directly used for evaluating the acidification process in the external anode mortar under the applied external current. The influence of the applied external current on the acidification process in the external anode mortar was also investigated and will be reported elsewhere. The experiment results presented in this paper will be also used to distinguish the consumption of OH^- ions in mortar pore solution and CH in the mortar matrix, and to further discuss the detail acidification process in the external anode mortar during ICCP treatment.

5. Conclusion

In this study, the acidification effect in simulated concrete pore solutions under ICCP treatment was characterized. The main conclusions are summarized as follows:

(1) The applied external current led to a slightly reduced corrosion resistance of the primary Ti mesh anode. This effect increased the corrosion current density of Ti mesh, leading to a more severe propagation of products on its surface.

(2) pH value of the simulated concrete pore solution in the anode cell decreased under the applied external current, and this negative effect was more pronounced with a higher applied current density. The presence of chlorides in simulated concrete pore solution accelerated the consumption rate of OH^- ions in the solutions, indicating a more pronounced acidification effect under marine environment.

(3) The relationship between OH^- concentration (c_{OH^-}) in simulated concrete pore solution near Ti mesh anode and accumulative electric charge quantity Q during ICCP treatment met Logistic regression model. For the chloride-free simulated concrete pore solution, the relationship between c_{OH^-} and Q can be expressed as: $c = \frac{c_0}{1+\left(Q/81.941\right)^{2.365}}$; for the chloride-containing simulated concrete pore solution, the relationship between c_{OH^-} and Q can be expressed as: $c = \frac{c_0}{1+\left(Q/72.319\right)^{3.122}}$.

Based on the above equations, the acidification effect induced by ICCP treatment in simulated concrete pore solution can be quantitatively evaluated.

Acknowledgments

This work was financially supported by National Key R & D Program of China (No. 2017YFB0309904), National Natural Science Foundation of China (No. 51572088 and 51602050), Pearl River S&T Nova Program of Guangzhou (No. 201806010188) and State Key Laboratory of Silicate Materials for Architectures (Wuhan University of Technology, No. SYSJJ2017-05). Their financial supports are gratefully acknowledged.

Conflict of interest

All authors declare no conflict of interest in this paper.

References

1. R. B. Polder, W. H. A. Peelen and M. Raupach, Economic effects of full corrosion surveys for aging concrete structures, *Mater. Corros.*, **64** (2013), 105–110.
2. G. Campione, F. Cannella, L. Cavaleri, et al., Moment-axial force domain of corroded R.C. columns, *Mater. Struct.*, **50** (2017), 21.
3. M. M. Mennucci, E. P. Banczek, P. R. P. Rodrigues, et al., Evaluation of benzotriazole as corrosion inhibitor for carbon steel in simulated pore solution, *Cem. Concr. Comp.*, **31** (2009), 418–424.
4. K. C. Clear, Measuring rate of corrosion of steel in field concrete structures, Washington: *Transportation Research Board*, 1989.
5. D. V. Val, Deterioration of strength of RC beams due to corrosion and its influence on beam reliability, *ASCE J. Struct. Eng.*, **133** (2007), 1297–1306.
6. G. Campione, F. Cannella and L. Cavaleri, Shear and flexural strength prediction of corroded R.C. beams, *Constr. Build. Mater.*, **149** (2017), 395–405.
7. L. Bertolini, B. Elsener, P. Pedeferri, et al., *Corrosion of steel in concrete: prevention, diagnosis, repair*. John Wiley & Sons, 2013.
8. S. Pour-Ali, C. Dehghanian and A. Kosari, Corrosion protection of the reinforcing steels in chloride-laden concrete environment through epoxy/polyaniline-camphorsulfonate nanocomposite coating, *Corros. Sci.*, **90** (2015), 239–241.
9. X. Zhou, H. Yang and F. Wang, Investigation on the inhibition behavior of a pentaerythritol glycoside for carbon steel in 3.5% NaCl saturated $Ca(OH)_2$ solution, *Corros. Sci.*, **54** (2012), 193–195.
10. J. Carmona, P. Garcés and M. A. Climent, Efficiency of a conductive cement-based anodic system for the application of cathodic protection, cathodic prevention and electrochemical chloride extraction to control corrosion in reinforced concrete structures, *Corros. Sci.*, **96** (2015), 102–106.
11. P. Pedeferri, Cathodic protection and cathodic prevention, *Constr. Build. Mater.*, **10** (1996), 391.

12. D. A. Koleva, Corrosion and protection in reinforced concrete Pulse cathodic protection: an improved cost-effective alternative, Ph.D Thesis, TU Delft, The Netherlands, 2007.
13. C. J. Weale, Cathodic protection of reinforced concrete: anodic processes in cement and related electrolytes, Ph.D Thesis, Aston University, United Kingdom, 1992.
14. C. Christodoulou, G. Glass, J. Webb, et al., Assessing the long term benefits of impressed current cathodic protection, *Corros. Sci.*, **52** (2010), 2671–2679.
15. K. Wilson, M. Jawed and V. Ngala, The selection and use of cathodic protection systems for the repair of reinforced concrete structures, *Constr. Build. Mater.*, **39** (2013), 19–23.
16. B. Elsener, Long-term durability of electrochemical chloride extraction, *Mater. Corros.*, **59** (2008), 91–97.
17. J. Xu and W. Yao, Current distribution in reinforced concrete cathodic protection system with conductive mortar overlay anode, *Constr. Build. Mater.*, **23** (2009), 2220–2226.
18. L. Bertolini, F. Bolzoni and T. Pastore, Effectiveness of a conductive cementitious mortar anode for cathodic protection of steel in concrete, *Cem. Concr. Res.*, **34** (2004), 681–684.
19. L. Bertolini, F. Bolzoni and P. Pedeferri, Cathodic protection and cathodic prevention in concrete: principles and applications, *J. App. Electrochem.*, **28** (1998), 1321–1323.
20. H. McArthur, S. D'Arcy and T. Barker, Cathodic protection by impressed DC currents for construction, maintenance and refurbishment in reinforced concrete, *Constr. Build. Mater.*, **7** (1993), 85–88.
21. W. H. A. Peelen, R. B. Polder and E. Redaelli, Qualitative model of concrete acidification due to cathodic protection, *Mater. Corros.*, **59** (2008), 81–84.
22. W. Green, F. Andrews-Phaedonos, G. Brewster, et al., Lynch's Bridge: a case study in the cathodic protection of reinforced concrete, *41st Australasian Corrosion Association Conference*, Newcastle, New South Wales, Australia 18-21 November 2011.
23. P. Ghods, O. B. Isgor and G. Mcrae, The effect of concrete pore solution composition on the quality of passive oxide films on black steel reinforcement, *Cem. Concr. Compos.*, **31** (2009), 2–7.
24. A. Leemann, B. Lothenbach and C. Thalmann, Influence of superplasticizers on pore solution composition and on expansion of concrete due to alkali-silica reaction, *Constr. Build. Mater.*, **25** (2011), 344–348.
25. M. Moreno, W. Morris and M. G. Alvarez, Corrosion of reinforcing steel in simulated concrete pore solutions: Effect of carbonation and chloride content, *Corros. Sci.*, **46** (2004), 2681–2685.
26. M. Saremi and E. Mahallati, A study on chloride-induced depassivation of mild steel in simulated concrete pore solution, *Cem. Concr. Res.*, **32** (2002), 1915–1921.
27. F. Zhang, J. Pan and C. Lin, Localized corrosion behaviour of reinforcement steel in simulated concrete pore solution, *Corros. Sci.*, **51** (2009), 2130–2133.
28. J. Xu and W. Yao, Electrochemical studies on the performance of conductive overlay material in cathodic protection of reinforced concrete, *Constr. Build. Mater.*, **25** (2011), 2655–2631.
29. D. A. Koleva, J. H. W. de Wit, K. van Breugel, et al., Investigation of corrosion and cathodic protection in reinforced concrete: I. Application of electrochemical techniques interdisciplinary topics, *J. Electrochem. Soc.*, **154** (2007), 52–55.